Physica B 688 (2024) 416124

Contents lists available at ScienceDirect

Physica B: Condensed Matter

journal homepage: www.elsevier.com/locate/physb

Micromagnetic modeling of double spin-torque magnetic tunnel junction devices

B. Pruckner [a,*], S. Fiorentini [c], W. Goes [c], S. Selberherr [b], V. Sverdlov [a,b]

[a] Christian Doppler Laboratory for Nonvolatile Magnetoresistive Memory and Logic at the Institute for Microelectronics, TU Wien, Gußhausstraße 27-29/E360, 1040 Vienna, Austria

[b] Institute for Microelectronics, TU Wien, Gußhausstraße 27-29/E360, 1040 Vienna, Austria

[c] Silvaco Europe Ltd. Cambridge, United Kingdom

ARTICLE INFO

Keywords:
Spin and charge drift–diffusion
Spin-transfer torque
Magnetic tunnel junctions
STT-MRAM
Double spin-torque MTJ

ABSTRACT

Emerging nonvolatile magnetoresistive random access memory exhibits high endurance and long data retention compared to flash memory. Additionally, devices with double spin torque magnetic tunnel junctions (dsMTJ) featuring two magnetic reference layers demonstrate enhanced torques, fast switching, and reduced switching currents. To accurately model these devices, we adopt a coupled spin and charge transport approach allowing to describe spin-transfer torques in metallic spin valves and magnetic tunnel junctions on equal footing. Our findings indicate the critical influence of metallic non-magnetic spacers (NMS) properties separating the free layer from the second reference layer on the switching speed improvement in dsMTJ devices.

1. Introduction

Spin-transfer torque magnetoresistive random access memory (STT-MRAM) has emerged as a promising nonvolatile memory technology which offers scalability, high endurance, and faster operation compared to flash memory [1,2]. Its ability to compete with SRAM has the potential to revolutionize future information storage. The core of an MRAM cell is a magnetic tunnel junction (MTJ) consisting of a CoFeB magnetic reference layer (RL), an MgO tunnel barrier (TB), and a CoFeB free magnetic layer (FL). A device with perpendicularly magnetized FL and RL (pMTJ) enables considerable footprint reduction and opens a path to high density MRAM solutions. There have been continuous efforts to enhance the switching performance of STT-MRAM devices, with the aim of achieving sub-nanosecond (sub-ns) switching times. While spin–orbit torque (SOT) devices have shown sub-ns switching performance, their three-terminal device structure is not ideal from a technological standpoint compared to the two-terminal structure of STT devices [3]. The incorporation of molybdenum (Mo) in pMTJ devices has shown to outperform regular Ta-based pMTJ, whereas Ta acts as the buffer/cap of the CoFeB electrodes, in terms of perpendicular magnetic anisotropy (PMA), thermal tolerance, and switching performance [4].

Double magnetic tunnel junctions (DMTJ), a MTJ with an additional RL and a second TB, have been investigated as efficient alternative to regular MTJ devices, with up to two-times increased switching efficiency [5,6]. However, the structure leads to lower TMR values, due to the second TB diluting the main barrier's TMR signal, which complicates efficient reading of magnetic states of the DMTJ [7]. A novel device structure with an additional reference layer (RL_2) positioned on top of the traditional pMTJ has recently been proposed, resulting in a double spin-torque magnetic tunnel junction (dsMTJ) [8], offering a significant increase in switching performance compared to pMTJs with a single RL.

Accurate modeling of advanced MRAM cells requires evaluating spin currents and torques in MTJs with multiple RLs separated from the FL by a TB or a normal metal non-magnetic spacer (NMS). In this work, we use the spin-charge drift–diffusion approach proposed in [9] to evaluate spin torques in multilayered structures, enabling the investigation of dsMTJ devices and the role of nonmagnetic metal spacers to optimize switching currents and speeds. This self-consistent approach goes beyond standard phenomenological approaches, by unifying spin torque contributions from the tunnel barrier interface, proposed by Slonczewski [10], and contributions acting in the bulk, proposed by Zhang-Li [11]. Contributions to the torque from the TB and from the bulk of the structure are not independent [12]. The TB influences the spin currents impinging at the magnetization texture, in turn modifying the traditional bulk Zhang-Li torque contribution. Therefore a unified treatment of the effects due to TB polarization and FL magnetization texture on the spin accumulation is required.

* Corresponding author.
E-mail address: pruckner@iue.tuwien.ac.at (B. Pruckner).

https://doi.org/10.1016/j.physb.2024.416124
Received 30 July 2023; Received in revised form 14 April 2024; Accepted 19 May 2024
Available online 30 May 2024

2. Method

We employ a fully three-dimensional finite element method (FEM) based modeling and simulation approach [9], which includes all physical phenomena responsible for proper dsMTJ operation. We employ the Landau–Lifshitz–Gilbert (LLG) equation to describe the dynamics of the magnetization.

$$\frac{\partial \mathbf{m}}{\partial t} = -\gamma \mathbf{m} \times \mathbf{H}_{\text{eff}} + \alpha \mathbf{m} \times \frac{\partial m}{\partial t} + \frac{1}{M_S}\mathbf{T}_S \tag{1}$$

Here $\mathbf{m} = \mathbf{M}/M_S$ is the local normalized magnetization, where M_S is the saturation magnetization. α is the Gilbert damping factor and γ the gyromagnetic ratio. The effective field $\mathbf{H}_{\text{eff}}$ encompasses the magnetic anisotropy field, the exchange field, and the demagnetization field. To evaluate the demagnetization field contribution only in the disconnected magnetic domains, we utilize a hybrid approach which combines the boundary element method and the finite element method (FEM-BEM) [13]. While the applied micromagnetic model allows domain wall formation in the FL during magnetization reversal, in the structures investigated in this work, with a FL thickness of 1.35 nm and a diameter of 20 nm, near-uniform rotation of the magnetization is present. To correctly describe the switching behavior of dsMTJ devices a complete description of the torque $\mathbf{T}_S$ is obtained from the non-equilibrium spin accumulation $\mathbf{S}$ acting on the magnetization via the exchange interaction.

$$\mathbf{T}_S = -\frac{D_e}{\lambda_J^2}\mathbf{m} \times \mathbf{S} - \frac{D_e}{\lambda_\varphi^2}\mathbf{m} \times (\mathbf{m} \times \mathbf{S}) \tag{2}$$

λ_J is the exchange length, λ_φ is the spin dephasing length, and D_e is the electron diffusion coefficient inside the ferromagnetic layers. A coupled spin and charge drift–diffusion (DD) formalism is used to accurately describe the behavior of the non-equilibrium spin accumulation $\mathbf{S}$.

$$D_e\left(\frac{\mathbf{S}}{\lambda_{sf}^2} + \frac{\mathbf{S} \times \mathbf{m}}{\lambda_J^2} + \frac{\mathbf{m} \times (\mathbf{S} \times \mathbf{m})}{\lambda_\varphi^2}\right) = -\nabla \cdot \overline{\mathbf{J}_S} \tag{3}$$

$$\overline{\mathbf{J}_S} = -\frac{\mu_B}{e}\beta_\sigma\left(\overline{\mathbf{J}_C} \otimes \mathbf{m} + \beta_D D_e \frac{e}{\mu_B}[(\nabla \mathbf{S})\mathbf{m}] \otimes \mathbf{m} - D_e \nabla \mathbf{S}\right) \tag{4}$$

$$\mathbf{J}_C = \sigma \mathbf{E} - \beta_D D_e \frac{e}{\mu_B}[(\nabla \mathbf{S})\mathbf{m}] \tag{5}$$

$\mathbf{J}_C$ is the charge current density in multi-layered structures with ferromagnetic and non-magnetic layers, and TBs. The first term in (5) is Ohm's law and the second term is the magnetoresistance contribution in ferromagnetic layers. σ is the conductivity, β_D is the diffusion polarization, D_e is the diffusion constant, and $\mathbf{E}$ is the electric field. $(\nabla \mathbf{S})$ is the vector gradient of the spin accumulation $\mathbf{S}$. $\overline{\mathbf{J}_S}$ is the spin current tensor for multilayer structures with ferromagnetic and non-magnetic layers. λ_{sf} is the spin–flip length, μ_B is the Bohr magneton, and β_σ is the conductivity polarization. The first and second term in (4) describe the contribution from polarized currents in ferromagnetic layers and the third term describes the diffusion of spins. The magnetization dynamics typically happen at a timescale three orders of magnitude slower than spin dynamics [14], the spin accumulation is assumed to immediately relax to the current magnetization state. By employing continuous boundary conditions [15] for the spin accumulation and spin current densities at the interfaces between the ferromagnet and non-magnetic spacer (NMS), the DD formalism allows for the correct description of spin and charge transport in spin valve structures, with a NMS between two ferromagnetic layers. To extend this method to MTJs, the tunnel barrier is modeled as a poor conductor with a local conductance $\sigma(\theta)$ which depends on the angle θ between the local magnetization directions of the adjacent ferromagnetic layers [9].

$$\sigma(\theta) = \frac{\sigma_P + \sigma_{AP}}{2}\left(1 + \left(\frac{\text{TMR}}{2 + \text{TMR}}\right) cos\theta\right) \tag{6}$$

σ_P (σ_{AP}) is the conductance in the parallel (anti-parallel) state and TMR is the tunneling magnetoresistance ratio. The charge and spin current flow through a TB can be expressed by using the non-equilibrium Green's function formalism [16]. This can be simplified to following boundary condition at the TB interfaces, which can describe the spin transport through a TB correctly [9]. The boundary condition defines the spin current at either interface of the TB. This way the flow of spin current through the TB can be described.

$$\mathbf{J}_{S,TB} = -\frac{\mu_B}{e}\frac{\mathbf{J}_C \cdot \mathbf{n}}{1 + P_{RL}P_{FL}\mathbf{m}_{RL} \cdot \mathbf{m}_{FL}}\left[P_{RL}\mathbf{m}_{RL} + P_{FL}\mathbf{m}_{FL} + 1/2(P_{RL}P_{RL}^{\eta} - P_{FL}P_{FL}^{\eta})\mathbf{m}_{RL} \times \mathbf{m}_{FL}\right] \tag{7}$$

P_{RL}, P_{FL} are the in-plane Slonczewski interface polarization parameters, and $P_{RL}^{\eta}, P_{FL}^{\eta}$ are the out-of-plane interface polarization parameters. $\mathbf{J}_C \cdot \mathbf{n}$ is the interface-normal component of the charge current. $\mathbf{m}_{RL}$ and $\mathbf{m}_{FL}$ are the normalized magnetization vectors of the RL and FL, respectively.

We expand the promising Mo-based pMTJ device structure [4] by adding a second RL_2 and a NMS as shown in Fig. 1, and apply our micromagnetic model to the resulting dsMTJ structure to investigate the spin torques acting in the magnetic layers as well as the switching performance of both pMTJ and dsMTJ. Material parameters are shown in Table 1.

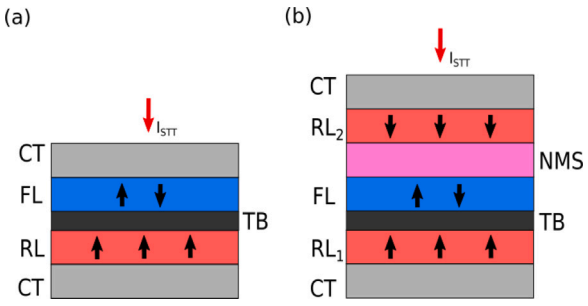

Fig. 1. Schematic of an (a) MTJ with the ferromagnetic RL and FL separated by a TB and contact layers (CT) at top and bottom and (b) dsMTJ with an additional RL and a NMS on top of the MTJ. The STT current is applied in the direction of the stack. The magnetization of the layers is depicted as black arrows.

Table 1
Material and simulation parameters of the pMTJ and dsMTJ devices.

TB thickness	0.9 nm
FL thickness	1.35 nm
RL_1 thickness	1.0 nm
RL_2 thickness	1.0 nm
NMS thickness	1.0 nm
Stack diameter	20 nm
TMR	0.65
Saturation magnetization, M_S	$8.1 \cdot 10^5$ A/m
Anisotropy constant, K	$7.34 \cdot 10^5$ J/m^3
Damping constant, α	0.02
Conductivity polarization, β_σ	0.52
Diffusivity polarization, β_D	0.7
Diffusion coefficient ferromagnet $CoFeB$, $D_{e,FM}$	$2 \cdot 10^{-3}$ m^2/s
Conductivity ferromagnet $CoFeB$, σ_{FM}	$4 \cdot 10^6$ S/m
Conductivity Ta, σ_{Ta}	$5 \cdot 10^5$ S/m
Conductivity Ru, σ_{Ru}	$1.5 \cdot 10^6$ S/m
Spin dephasing length, λ_φ	0.4 nm
Spin exchange length, λ_J	1 nm
Spin–flip length ferromagnet $CoFeB$, $\lambda_{SF,FM}$	10 nm
Spin–flip length Ta, $\lambda_{SF,Ta}$	1.9 nm
Spin–flip length Ru, $\lambda_{SF,Ru}$	4.0 nm

3. Enhancing the performance of STT-MRAM

The dsMTJ architecture harnesses additional spin torque coming from the second RL_2, while the TMR remains unchanged compared to regular MTJ devices, thus enabling increased speed and improved efficiency in the switching process [8,17]. For the spin torques coming

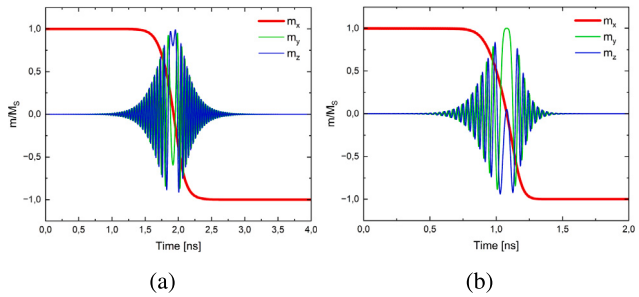

Fig. 2. The normalized magnetization during the switching process for (a) a pMTJ and (b) a dsMTJ with a ruthenium non-magnetic spacer. A current density of 8 MA/cm^2 is applied.

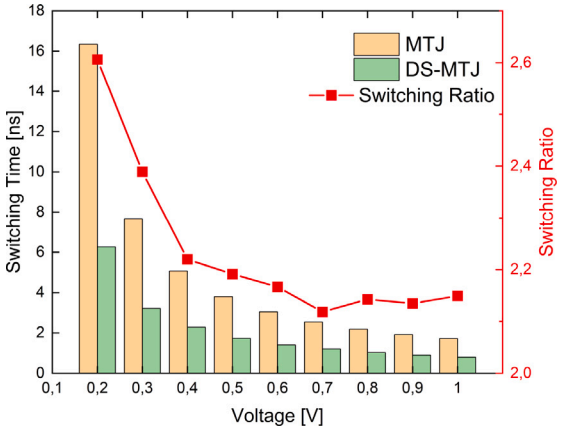

Fig. 3. Switching times for a pMTJ and dsMTJ with a Ru-NMS for different applied voltages. The switching ratio gives the acceleration of the switching process in a dsMTJ device compared to a pMTJ.

from both RLs to add up, the magnetizations of RL_1 and RL_2 have to be antiparallel to each other. The additional spin current from RL_2 impinging the FL leads to a higher total spin torque acting on the magnetization. Fig. 2 shows the normalized magnetization $\mathbf{m}/M_S$, with the saturation magnetization M_S, of the FL in both, a pMTJ and a dsMTJ with a ruthenium (Ru) NMS. A perpendicular-to-plane STT-current of $I_{STT} = 8$ MA/cm^2 was applied in both cases. Under equal conditions, the dsMTJ structure shows a two-times faster switching behavior than an pMTJ.

Fig. 3 shows the switching time of a pMTJ and a dsMTJ with Ru as NMS material for different voltages, as well as the switching time ratio. An enhancement of the switching performance of around two times in the dsMTJ device compared to the one in the regular pMTJ device was achieved. We show a clearly faster switching of the dsMTJ device for all applied voltages, as well as reaching the sub-ns domain for switching, in agreement with the experiment [8].

Fig. 4 shows the switching current of a pMTJ and a dsMTJ with Ru-NMS and a dsMTJ with a Ta-NMS, in dependence of the applied voltage pulse length. We observe a slight reduction of the switching current in the Ta-dsMTJ and a significant reduction in the Ru-dsMTJ device compared to the pMTJ. For a 10 ns voltage pulse the results show a two-times reduction in critical switching current in the Ru-dsMTJ compared to the regular pMTJ, in agreement with [8], highlighting not only the performance of the dsMTJ structure but also the importance of the material of the NMS layer, which will be further elaborated below.

Heating has been shown to play an important role in STT-MTJ switching, leading to smaller switching times but also less reliable

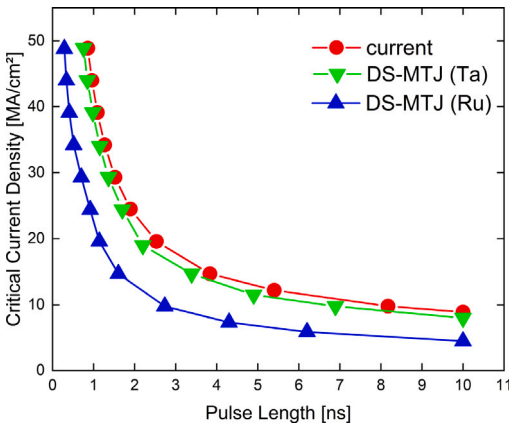

Fig. 4. Switching currents for various pulse lengths for a pMTJ and dsMTJs with a Ta-NMS and a Ru-NMS, from an anti-parallel to a parallel magnetic state.

switching [18,19]. The reliability under thermal fluctuations is described by the thermal stability factor Δ [20]

$$\Delta = \frac{M_S H_{k,eff} V}{2 k_B T.} \tag{8}$$

The thermal stability factor for the FL of the structures investigated in this work is estimated to be $\Delta \approx 75$. Due to the significant lower switching currents, dsMTJ devices experience much less heating than regular MTJ devices and therefore exhibit less thermal instability at comparable switching times.

Results of the switching time enhancement from P to AP and from AP to P states in a pMTJ and dsMTJ with Ta and Ru as NMS material are shown in Fig. 5. The results for Ru display a significant switching time acceleration compared to a pMTJ without the second reference layer RL_2, in agreement with earlier simulations [21] and experimental results [17]. For a Ta spacer, however, the advantage in switching acceleration due to the second RL is only several percent and disappears at higher bias voltages. In order to explain this behavior, the torques acting on the FL are plotted in Fig. 6. The magnetization direction in the ferromagnetic layers is depicted by black arrows and the FL is orthogonal to the RLs. The damping-like component of the spin torque inside the FL shows a large peak at the TB interface and a smaller additional peak at the NMS interface coming from RL_2. It is clearly visible that the torque contribution due to the second RL_2 is large in the case of a Ru NMS.

In Fig. 5 a change in switching behavior of parallel to antiparallel (P→AP) and antiparallel to parallel (AP→P) switching can be observed. While for the pMTJ AP→P switching shows faster switching times than P→AP switching, this is reversed in both the Ta-dsMTJ and the Ru-dsMTJ. This change in switching behavior is influenced by the stray field of the second RL, which acts against magnetization switching in an antiparallel configuration and supports magnetization switching in a parallel configuration.

The spin–flip length λ_{SF}, which governs the decay of the longitudinal components of the spin accumulation, in Ru is 4.0 nm and is more than two times larger than in Ta (1.9 nm). Therefore, the spin accumulation impinging from RL_2 to the FL decays significantly in Ta compared to Ru, which results in a much weaker contribution of the second RL_2 to the torque (Fig. 6) and the switching time acceleration, in agreement with Fig. 5. To further investigate the dependence of the switching efficiency on the NMS material, we investigated the spin torque acting in the FL while varying λ_{SF} of the NMS. In Fig. 7 the total spin torque in the FL is plotted for different λ_{SF} of a 1 nm thick NMS. Clearly visible is a rapid increase in total spin torque for λ_{SF} in the range from 0 to 5 nm. This behavior explains the much better switching performance of the investigated dsMTJ structures with a Ru spacer compared to a Ta spacer.

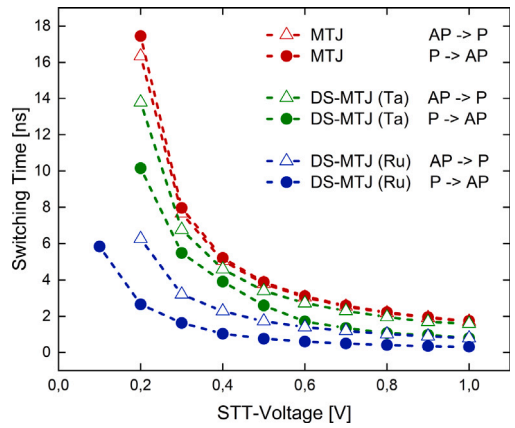

Fig. 5. Switching times of a pMTJ and dsMTJ with different NMS materials, for parallel to antiparallel (P→AP) and antiparallel to parallel (AP→P) configuration.

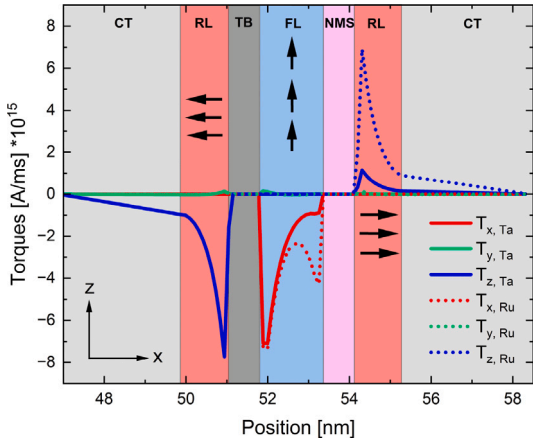

Fig. 6. Spin torque components acting in the layers of a dsMTJ device. The magnetization direction is -x in RL_1 on the left, +x in RL_2 on the right and +z in the FL. The torques are shown for Ta and Ru as materials of the NMS layer.

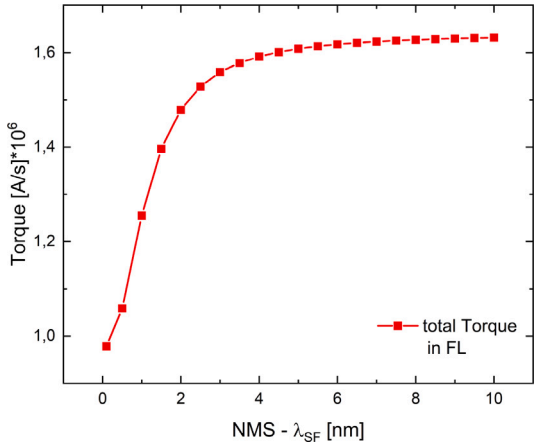

Fig. 7. The total spin torque acting in the free layer of the dsMTJ for different spin–flip lengths λ_{SF} of the NMS layer.

4. Conclusion

We use a fully three-dimensional FEM based micromagnetic model based on a coupled spin-and-charge drift–diffusion approach to calculate the spin torque acting in multilayer structures and to simulate the switching behavior of MTJ devices. We extend the perpendicularly magnetized MTJ structure by adding a second ferromagnetic reference layer and a non-magnetic spacer on top to achieve a double-spin torque MTJ structure. We show that the experimentally reported two-times enhancement of switching performance is indeed attributed to the additional spin torque coming from the second reference layer acting in the free layer, in case the two reference layers are magnetized antiparallel to each other. We demonstrate that the efficiency of switching of a dsMTJ heavily depends on the material of the non-magnetic spacer. This is due to the amount of additional spin torque acting in the free layer being determined by the spin–flip length λ_{SF} of the non-magnetic spacer. Higher λ_{SF} leads to higher values of spin torque in the free layer and thus to an increased switching performance. Materials with large spin–flip lengths like Ru (λ_{SF} = 4.0 nm) are promising candidates for non-magnetic spacer layers, as opposed to Ta with a shorter spin–flip length and inferior switching performance.

CRediT authorship contribution statement

B. Pruckner: Conceptualization, Data curation, Formal analysis, Investigation, Methodology, Visualization, Writing – original draft, Writing – review & editing. **S. Fiorentini:** Conceptualization, Resources, Software. **W. Goes:** Software, Validation. **S. Selberherr:** Conceptualization, Supervision, Validation. **V. Sverdlov:** Conceptualization, Funding acquisition, Methodology, Project administration, Resources, Supervision, Validation.

Declaration of competing interest

The authors declare that they have no known competing financial interests or personal relationships that could have appeared to influence the work reported in this paper.

Data availability

Data will be made available on request.

Acknowledgments

The financial support by the Federal Ministry of Labor and Economy, the National Foundation for Research, Technology and Development, and the Christian Doppler Research Association, Austria is gratefully acknowledged. The authors acknowledge TU Wien Bibliothek, Austria for financial support through its Open Access Funding Program.

References

[1] T.Y. Lee, J.M. Lee, M.K. Kim, J.S. Oh, J.W. Lee, H.M. Jeong, P.H. Jang, M.K. Joo, K. Suh, S.H. Han, D.-E. Jeong, T. Kai, J.H. Jeong, J.-H. Park, J.H. Lee, Y.H. Park, E.B. Chang, Y.K. Park, H.J. Shin, Y.S. Ji, S.H. Hwang, K.T. Nam, B.S. Kwon, M.K. Cho, B.Y. Seo, Y.J. Song, G.H. Koh, K. Lee, J.-H. Lee, G.T. Jeong, World-most energy-efficient MRAM technology for non-volatile RAM applications, in: International Electron Devices Meeting, IEDM, 2022, pp. 10.7.1–10.7.4.

[2] S. Ikegawa, K. Nagel, F.B. Mancoff, S.M. Alam, M. Arora, M. DeHerrera, H.K. Lee, S. Mukherjee, G. Shimon, J.J. Sun, I. Rahman, F. Neumeyer, H.Y. Chou, C. Tan, A. Shah, S. Aggarwal, High-speed (400MB/s) and low-BER STT-MRAM technology for industrial applications, in: International Electron Devices Meeting, IEDM, 2022, pp. 10.4.1–10.4.4.

[3] C. Safranski, G. Hu, J.Z. Sun, P. Hashemi, S.L. Brown, L. Buzi, C.P. D'Emic, E.R.J. Edwards, E. Galligan, M.G. Gottwald, O. Gunawan, S. Karimeddiny, H. Jung, J. Kim, K. Latzko, P.L. Trouilloud, D.C. Worledge, Reliable sub-nanosecond switching in magnetic tunnel junctions for MRAM applications, IEEE Trans. Electron Devices 69 (12) (2022) 7180–7183.

[4] D. Lyu, P. Khanal, Y. Lv, B. Zhou, H. Yun, Q. Jia, B.R. Zink, Y. Fan, K.A. Mkhoyan, W. Wang, J.-P. Wang, Sub-ns switching and cryogenic-temperature performance of Mo-based perpendicular magnetic tunnel junctions, IEEE Electron Device Lett. 43 (8) (2022) 1215–1218.

[5] G. Hu, J.H. Lee, J.J. Nowak, J.Z. Sun, J. Harms, A. Annunziata, S. Brown, W. Chen, Y.H. Kim, G. Lauer, L. Liu, N. Marchack, S. Murthy, E.J. O'Sullivan, J.H. Park, M. Reuter, R.P. Robertazzi, P.L. Trouilloud, Y. Zhu, D.C. Worledge, STT-MRAM with double magnetic tunnel junctions, in: 2015 IEEE International Electron Devices Meeting, IEDM, 2015, pp. 26.3.1–26.3.4.

[6] P.-Y. Clément, C. Baraduc, M. Chshiev, B. Diény, L. Vila, C. Ducruet, Double barrier magnetic tunnel junctions with write/read mode select layer, in: 2014 IEEE 6th International Memory Workshop, IMW, 2014, pp. 1–4.

[7] D. Sanchez Hazen, B.M.S. Teixeira, D. Salomoni, S. Auffret, L. Vila, R.C. Sousa, I.L. Prejbeanu, L.D. Buda-Prejbeanu, B. Dieny, Real time investigation of double magnetic tunnel junction with a switchable assistance layer for high efficiency STT-MRAM, APL Mater. 10 (3) (2022) 031104.

[8] G. Hu, G. Lauer, J.Z. Sun, P. Hashemi, C. Safranski, S.L. Brown, L. Buzi, E.R.J. Edwards, C.P. D'Emic, E. Galligan, M.G. Gottwald, O. Gunawan, H. Jung, J. Kim, K. Latzko, J.J. Nowak, P.L. Trouilloud, S. Zare, D.C. Worledge, 2X reduction of STT-MRAM switching current using double spin-torque magnetic tunnel junction, in: International Electron Devices Meeting, IEDM, 2021, pp. 2.5.1–2.5.4.

[9] S. Fiorentini, M. Bendra, J. Ender, R.L. Orio, W. Goes, S. Selberherr, V. Sverdlov, Spin and charge drift-diffusion in ultra-scaled MRAM cells, Sci. Rep. 12 (2022) 20958.

[10] J. Slonczewski, Current-driven excitation of magnetic multilayers, J. Magn. Magn. Mater. 159 (1) (1996) L1–L7.

[11] S. Zhang, Z. Li, Roles of nonequilibrium conduction electrons on the magnetization dynamics of ferromagnets, Phys. Rev. Lett. 93 (2004) 127204.

[12] S. Fiorentini, B. Pruckner, W. Goes, S. Selberherr, V. Sverdlov, Roles of nonequilibrium conduction electrons on the magnetization dynamics of ferromagnets, ECS Trans. 111 (2023) 181–186.

[13] J. Ender, M. Mohamedou, S. Fiorentini, R.L. Orio, S. Selberherr, W. Goes, V. Sverdlov, Efficient demagnetizing field calculation for disconnected complex geometries in STT-MRAM cells, in: SISPAD Conference, 2020, pp. 213–216.

[14] S. Zhang, P.M. Levy, A. Fert, Mechanisms of spin-polarized current-driven magnetization switching, Phys. Rev. Lett. 88 (2002).

[15] C. Abert, M. Ruggeri, F. Bruckner, C. Vogler, A. Manchon, D. Praetorius, D. Suess, A self-consistent spin-diffusion model for micromagnetics, Sci. Rep. 6 (2016) 16.

[16] M. Chshiev, A. Manchon, A. Kalitsov, N. Ryzhanova, A. Vedyayev, N. Strelkov, W.H. Butler, B. Dieny, Analytical description of ballistic spin currents and torques in magnetic tunnel junctions, Phys. Rev. B 92 (2015) 104422.

[17] G. Hu, C. Safranski, J.Z. Sun, P. Hashemi, S.L. Brown, J. Bruley, L. Buzi, C.P. D'Emic, E. Galligan, M.G. Gottwald, O. Gunawan, J. Lee, S. Karimeddiny, P.L. Trouilloud, D.C. Worledge, Double spin-torque magnetic tunnel junction devices for last-level cache applications, in: International Electron Devices Meeting, IEDM, 2022, pp. 10.2.1–10.2.4.

[18] T. Hadámek, S. Selberherr, W. Goes, V. Sverdlov, Asymmetry of current-induced heating in magnetic tunnel junctions, in: Book of Abstracts of the International Workshop on Computational Nanotechnology, Vol. 200, IWCN, 2021, pp. 49–50.

[19] T. Hadámek, S. Selberherr, W. Goes, V. Sverdlov, Modeling thermal effects in STT-MRAM, Solid-State Electron. 200 (2023) 108522.

[20] S. Ikeda, K. Miura, H. Yamamoto, K. Mizunuma, H.D. Gan, M. Endo, S. Kanai, J. Hayakawa, F. Matsukura, H. Ohno, A perpendicular-anisotropy CoFeB–MgO magnetic tunnel junction, Nat. Mater.als 9 (2010) 721–724.

[21] W.J. Loch, S. Fiorentini, N.P. Jørstad, W. Goes, S. Selberherr, V. Sverdlov, Double reference layer STT-MRAM structures with improved performance, Solid-State Electron. 194 (2022) 108373.